



# CHORUS

This is the accepted manuscript made available via CHORUS. The article has been published as:

## Pressure effects on the electronic structure and superconductivity of $(\text{TaNb})_{0.67}(\text{HfZrTi})_{0.33}$ high entropy alloy

K. Jasiewicz, B. Wiendlocha, K. Górnicka, K. Gofryk, M. Gazda, T. Klimczuk, and J. Tobola

Phys. Rev. B **100**, 184503 — Published 4 November 2019

DOI: [10.1103/PhysRevB.100.184503](https://doi.org/10.1103/PhysRevB.100.184503)

# Pressure effects on the electronic structure and superconductivity of $(\text{TaNb})_{0.67}(\text{HfZrTi})_{0.33}$ high entropy alloy

K. Jasiewicz,<sup>1</sup> B. Wiendlocha,<sup>1,\*</sup> K. Górnicka,<sup>2</sup> K. Gofryk,<sup>3</sup> M. Gazda,<sup>2</sup> T. Klimczuk,<sup>2</sup> and J. Tobola<sup>1</sup>

<sup>1</sup>*Faculty of Physics and Applied Computer Science,*

*AGH University of Science and Technology, Al. Mickiewicza 30, 30-059 Krakow, Poland*

<sup>2</sup>*Faculty of Applied Physics and Mathematics, Gdańsk University of Technology, ul. Narutowicza 11/12, 80-233 Gdańsk, Poland*

<sup>3</sup>*Idaho National Laboratory, Idaho Falls, Idaho 83415, USA*

(Dated: October 17, 2019)

Effects of pressure on the electronic structure, electron-phonon interaction, and superconductivity of the high entropy alloy  $(\text{TaNb})_{0.67}(\text{HfZrTi})_{0.33}$  are studied in the pressure range 0 - 100 GPa. The electronic structure is calculated using the Korringa-Kohn-Rostoker method with the coherent potential approximation. Effects of pressure on the lattice dynamics are simulated using the Debye-Grüneisen model and the Grüneisen parameter at ambient conditions. In addition, the Debye temperature and Sommerfeld electronic heat capacity coefficient were experimentally determined. The electron-phonon coupling parameter  $\lambda$  is calculated using the McMillan-Hopfield parameters and computed within the rigid muffin tin approximation. We find, that the system undergoes the Lifshitz transition, as one of the bands crosses the Fermi level at elevated pressures. The electron-phonon coupling parameter  $\lambda$  decreases above 10 GPa. The calculated superconducting  $T_c$  increases up to 40 - 50 GPa and, later, is stabilized at the larger value than for the ambient conditions, in agreement with the experimental findings. Our results show that the experimentally observed evolution of  $T_c$  with pressure in  $(\text{TaNb})_{0.67}(\text{HfZrTi})_{0.33}$  can be well explained by the classical electron-phonon mechanism.

## I. INTRODUCTION

High-pressure studies of superconducting materials have brought about the latest breakthrough in the field of superconductivity. The record-high  $T_c$  of 203 K in  $\text{H}_3\text{S}$ <sup>1</sup> and 250 K in  $\text{LaH}_{10}$ <sup>2</sup> at  $P > 150$  GPa were recently reported, and theoretical predictions show that even larger values of  $T_c$  are possible<sup>3,4</sup>. As superconductivity in these materials is mediated by the electron-phonon interaction, recent discoveries also turned attention to the effect of extreme pressure on superconductivity in other materials, including bulk conventional superconductors. This includes recent high-pressure studies on superconductivity in Nb-Ti alloy<sup>5</sup> and  $(\text{TaNb})_{0.67}(\text{HfZrTi})_{0.33}$  high-entropy alloy (HEA)<sup>6</sup>, on which we are focusing in the current work.

High entropy alloys<sup>7,8</sup> contain five or more elements and, due to stabilization by the configurational entropy, form simple "monoatomic" crystal structures such as cubic *bcc* or *fcc*, with statistical occupation of the single crystal site. The first superconducting HEA,  $\text{Ta}_{34}\text{Nb}_{33}\text{Hf}_8\text{Zr}_{14}\text{Ti}_{11}$ <sup>9</sup> was reported in 2014. It crystallizes in a *Im-3m* *bcc*-type of structure, with a lattice parameter of 3.36 Å. In this system, all atoms randomly occupy (2a) crystal site (on average). It is a type-II superconductor with the transition temperature of  $T_c = 7.3$  K. Experimental data as well as theoretical calculations<sup>10</sup> suggest conventional mechanism of superconductivity with a relatively strong electron phonon coupling parameter  $\lambda \sim 1$ . Several other examples of superconducting HEAs were later reported<sup>11-13</sup>, however, the  $\text{TaNbHfZrTi}$  family is still the most investigated one<sup>9,10,14,15</sup>. When the atomic concentration is slightly changed to  $\text{Ta}_{33.5}\text{Nb}_{33.5}\text{Hf}_{11}\text{Zr}_{11}\text{Ti}_{11}$ <sup>15</sup> [denoted

as  $(\text{TaNb})_{0.67}(\text{HfZrTi})_{0.33}$  or TNHZT in short], superconducting transition temperature slightly increases to 7.7 K. This alloy also hosts a cubic body-centered crystal structure, with the lattice parameter of 3.34 Å.

When the external pressure is applied,  $T_c$  of  $(\text{TaNb})_{0.67}(\text{HfZrTi})_{0.33}$  increases up to about 10 K at around 50-60 GPa and then it remains practically constant up to about 100 GPa. After that, it slightly decreases to 9 K at 190 GPa<sup>6</sup>. In our work we investigate effects of pressure on the electronic structure and superconductivity in this disordered system to better understand microscopic mechanisms controlling these interesting  $T_c(P)$  characteristics. As the crystal structure was determined experimentally to about 96 GPa<sup>6</sup> we perform our studies in the pressure range from 0 to 100 GPa. The electronic structure is calculated using the Korringa-Kohn-Rostoker method with the coherent potential approximation (KKR-CPA)<sup>16-19</sup>. From the KKR-CPA results, by using the rigid muffin tin approximation (RMTA),<sup>20</sup> the McMillan-Hopfield parameters are calculated. Effect of pressure on the lattice dynamics is simulated using the Debye model and Grüneisen parameter  $\gamma_G$ . To obtain  $\gamma_G$  it becomes necessary to determine the volume thermal expansion coefficient, thus experimental measurements of the crystal structure evolution with temperature were performed. Additionally, to assure the consistency of the analysis the low-temperature heat capacity was measured on the same sample to obtain  $T_c$ , Debye temperature  $\theta_D$ , and the Sommerfeld coefficient  $\gamma$ . As a final result, the pressure evolution of the electron-phonon coupling parameter  $\lambda(P)$  and the superconducting critical temperature  $T_c(P)$  are determined.

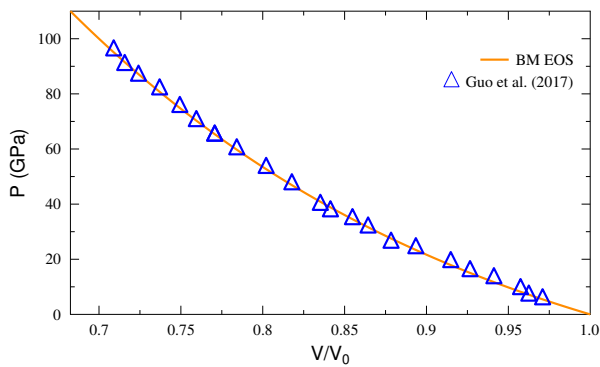


FIG. 1. Pressure dependence of the unit cell volume. Points correspond to the experimental data<sup>6</sup> and line is determined from the fitted Birch-Murnaghan equation of state.

## II. METHODOLOGY

### A. Synthesis & X-ray Crystallography

The  $\text{Ta}_{0.335}\text{Nb}_{0.335}\text{Hf}_{0.11}\text{Zr}_{0.11}\text{Ti}_{0.11}$  sample was prepared by melting the required high-purity elements, i.e., tantalum foil (99.9%), niobium pieces (99.99%), hafnium pieces (99.99%), zirconium foil (99.8%) and titanium pieces (99.99%). The elemental metals were arc-melted to a single metallic button under an argon atmosphere on a water-chilled copper plate. A piece of zirconium was used as a getter at each melting steps. After the initial melt, the sample nugget was turned and remelted three times to ensure the optimal mixing of the constituents. Mass loss during the synthesis was smaller than 1% and the resulting material was hard and silver in color.

The phase purity of the obtained material was checked by X-ray diffraction (XRD) using a Philips X'pert Pro MPD with Cu  $K_\alpha$  radiation. The sample exhibited ductility, and therefore could not be ground. **Because of that**, for qualitative and quantitative characterization the sample had to be converted into a plate form. In order to prepare the sample for the XRD analysis, the button was cut into smaller piece and then transformed into a plate using hydraulic press. The mechanical handling did not cause any sample contamination. The plate was put on the  $\text{Al}_2\text{O}_3$  (corundum) sample holder and mounted in a small furnace inside a diffractometer. Above  $400^\circ\text{C}$  the sample oxidizes and, hence, the XRD analysis in higher temperatures was not continued. The lattice parameter for TNHZT at different temperatures was estimated from the LeBail fit using a HighScore program.

### B. Heat capacity

Heat capacity measurements were carried out using a Quantum Design Physical Property Measurement System (PPMS) Evercool-II. The two- $\tau$  **relaxation** method

was used to measure the specific heat **without external magnetic field and under 8 T magnetic field**, in the temperature range 1.9 - 10 K. The sample was attached to the measuring stage **by** using Apiezon N grease to ensure good thermal contact.

### C. Electronic structure

Electronic structure calculations were performed using the Korringa-Kohn-Rostoker method with the coherent potential approximation (KKR-CPA)<sup>16-19</sup> to account for **atomic** disorder. Crystal potential of the muffin-tin type was constructed using the local density approximation (LDA), Perdew-Wang parametrization<sup>21</sup>, and in the semi-relativistic approach. Angular momentum cut-off was set to  $l_{max} = 3$ . Highly converged results were obtained for about 450  $\mathbf{k}$ -points grid in the irreducible part of Brillouin zone for self-consistent cycle and 2800  $\mathbf{k}$ -points for the densities of states (DOS) computations. Muffin-tin radius was set to the largest non-overlapping spheres (i.e.  $R_{MT} = a\sqrt{3}/4$ ) **and the** Fermi level ( $E_F$ ) was accurately determined from the generalized Lloyd formula<sup>17</sup>. **It is worth noting, that the KKR-CPA method has already been successfully applied to study different physical properties** of high entropy alloys<sup>22-25</sup>.

Electron-phonon coupling and its evolution under external pressure is studied using the so-called Rigid Muffin Tin Approximation (RMTA). **This method has been** successfully applied to many superconducting materials, mostly containing transition metal elements<sup>20,26-31</sup> and more recently, to the HEA  $\text{Ta}_{34}\text{Nb}_{33}\text{Hf}_8\text{Zr}_{14}\text{Ti}_{11}$ <sup>10</sup> at ambient pressure. In this approach, the electron-phonon interaction is decoupled into electronic and lattice contributions. **The** coupling parameter  $\lambda$  is computed as:

$$\lambda = \sum_i \frac{\eta_i}{M_i \langle \omega_i^2 \rangle}, \quad (1)$$

where  $\eta_i$  are the McMillan-Hopfield parameters<sup>32,33</sup> computed for each of the atom  $i$  in the unit cell,  $M_i$  is the atomic mass, and  $\langle \omega_i^2 \rangle$  is the properly defined average square atomic vibration frequency (see the discussion of the frequency moments in the Supplemental Material<sup>34</sup>). Within RMTA, McMillan-Hopfield parameters are calculated using the band-structure related quantities<sup>20,26,28</sup> employing expression:

$$\eta_i = \sum_l \frac{(2l+2)n_l(E_F)n_{l+1}(E_F)}{(2l+1)(2l+3)N(E_F)} \left| \int_0^{R_{MT}} r^2 R_l \frac{dV}{dr} R_{l+1} \right|^2, \quad (2)$$

where  $V(r)$  is the self-consistent potential at site  $i$ ,  $R_{MT}$  is the radius of the  $i$ -th MT sphere,  $R_l(r)$  is a regular solution of the radial Schrödinger equation (normalized to unity inside the MT sphere),  $n_l(E_F)$  is the  $l$ -th partial DOS per spin at the Fermi level  $E_F$ , and  $N(E_F)$  is the

total DOS per primitive cell and per spin. For a more detailed discussion of the approximations involved in this methodology, see e.g. Refs.<sup>28,29</sup> and references therein.

In the case of a random alloy, where a single crystal site  $i$  is occupied by several different atoms **that have** different concentrations, modification of Eq.(1) is necessary. In calculations of  $\lambda$  for binary alloys **having** similar atomic masses of elements (e.g. Nb-Mo), where one can expect similar denominators in Eq.(1) the McMillan-Hopfield parameters obtained from self-consistent KKR-CPA calculations, were simply weighted by atomic concentrations  $c_i$ <sup>35</sup>, **and were** predicting composition dependence of  $\lambda$  reasonably well. **Besides, in the** case of a monoatomic system **that** has a Debye-like phonon spectrum,  $\langle\omega_i^2\rangle$  may be reasonably well approximated using the experimental Debye temperature<sup>35-37</sup> as  $\langle\omega^2\rangle = \frac{1}{2}\theta_D^2$  (see Supplemental Material<sup>34</sup> for the derivation of this formula). That is especially useful in the present case of a multicomponent HEA, since it allows to estimate  $\lambda$  without knowledge of the phonon spectrum. As the Debye temperature represents the characteristic frequency of the whole system, we use it in combination with the concentration-weighted average atomic mass. **In this approach the** denominator in Eq. (1) takes the form:  $M_i\langle\omega_i^2\rangle \simeq \langle M\rangle\frac{1}{2}\theta_D^2$ , where  $\langle M\rangle = \sum_i c_i M_i$ . The final formula for the electron-phonon coupling (EPC) parameter  $\lambda$  of HEA used in our work becomes:

$$\lambda = \frac{\sum_i c_i \eta_i}{\frac{1}{2}\langle M\rangle\theta_D^2}, \quad (3)$$

where McMillan-Hopfield parameters  $\eta_i$  of each atom in the system are computed in the self-consistent KKR-CPA calculations **and**  $c_i$  is the atomic concentration of the element. As mentioned above, this approach was recently applied to the first superconducting high-entropy alloy  $\text{Ta}_{34}\text{Nb}_{33}\text{Hf}_8\text{Zr}_{14}\text{Ti}_{11}$ <sup>10</sup> at ambient pressure ( $T_c = 7.3$  K). The value of  $\lambda = 1.16$  was obtained in good agreement with the value of  $\lambda = 0.98$  determined from the renormalization of the electronic heat capacity coefficient  $\gamma$ . Here, the same approach is applied to  $(\text{TaNb})_{0.67}(\text{HfZrTi})_{0.33}$  system to study evolution of superconducting properties under pressure.

As far as the crystal structure is concerned, high pressure synchrotron X-ray diffraction measurements were performed in the pressure range from 0 to 96 GPa and **it was shown that**  $(\text{TaNb})_{0.67}(\text{HfZrTi})_{0.33}$  **maintains** the bcc structure, since no structural distortion was **observed**<sup>6</sup>. As there is no information on the crystal structure above this pressure we limit our studies to the pressure range from 0 to 100 GPa. Available experimental data of volume vs. pressure are shown in Fig. 1 and were fitted to the third order Birch-Murnaghan equation of state.<sup>38</sup>

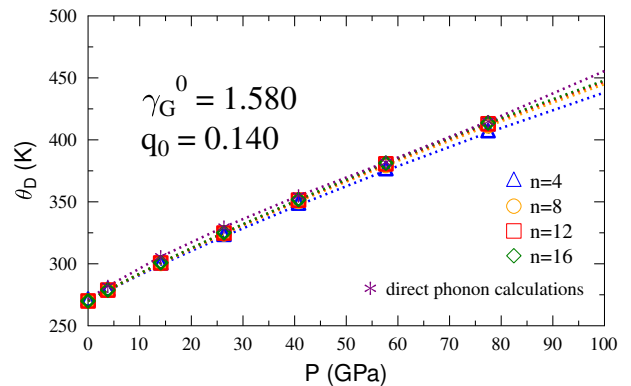


FIG. 2. Pressure dependence of  $\theta_D$  of niobium from the direct phonon calculations and from the Grüneisen model for several values of  $n$ .

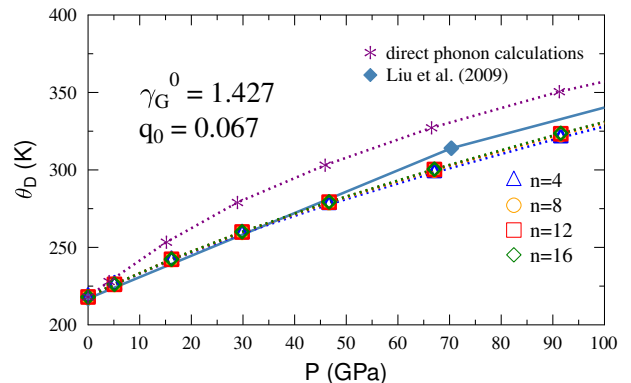


FIG. 3. Pressure dependence of  $\theta_D$  of tantalum from the direct phonon calculations, from the Grüneisen model for several values of  $n$ , and from the quasi-harmonic calculations of Liu *et al.*<sup>39</sup>.

$$P(V) = \frac{3}{2}B \left[ \left( \frac{V}{V_0} \right)^{-\frac{7}{3}} - \left( \frac{V}{V_0} \right)^{-\frac{5}{3}} \right] \left\{ 1 + \frac{3}{4}(B' - 4) \left[ \left( \frac{V}{V_0} \right)^{-\frac{2}{3}} - 1 \right] \right\}, \quad (4)$$

where  $V_0$  is the equilibrium volume. Bulk modulus of  $B = 177.35$  GPa and its derivative  $B' = 2.87$  were obtained and are used in the subsequent analysis.

#### D. Evolution of Debye temperature with pressure

The Debye temperature of TNHZT  $\theta_D^0$  was measured only at ambient conditions<sup>15</sup>, **therefore** it was also necessary to simulate its pressure dependence to calculate

$\lambda(P)$  and  $T_c(P)$  using Eq.(3). This can be performed using analytic model based on Grüneisen parameter  $\gamma_G$ <sup>40</sup> where

$$\gamma_G(V) = -\frac{\partial \ln \theta_D}{\partial \ln V}. \quad (5)$$

As the volume compression (in our case) reaches 30% (see, Fig. 1), a variation of Grüneisen parameter with pressure (volume) has to be taken into account. This can be done using the so-called second order Grüneisen parameter  $q$ :

$$q(V) = \frac{\partial \ln \gamma_G(V)}{\partial \ln V}, \quad (6)$$

which also may be pressure-dependent. Equations (5) and (6) cannot be solved in a simple way as both  $\gamma_G$  and  $q$  are volume-dependent parameters. Assuming that the next logarithmic derivative is constant:<sup>41</sup>

$$q'(V) = \frac{\partial \ln q(V)}{\partial \ln V} = \text{const.} \quad (7)$$

we may write  $q(V)$  as a power-law relation

$$q(V) = q_0 \zeta^n, \quad (8)$$

where  $\zeta = V/V_0$ ,  $n$  is a material-dependent constant parameter, and  $q_0 = q(V_0)$  is the value at ambient conditions. Such approximation leads to the formula for  $\gamma_G(V)$ <sup>42</sup>:

$$\gamma_G(V) = \gamma_G^0 e^{\left[\frac{q_0}{n}(\zeta^n - 1)\right]}. \quad (9)$$

Once  $\gamma_G(V)$  is calculated the Debye temperature for a given volume (or equivalently pressure) is computed from:

$$\theta_D(V) = \theta_D^0 \left(\frac{V}{V_0}\right)^{-\gamma_G(V)}. \quad (10)$$

Input parameters, required to compute  $\theta_D(V)$  are ambient-pressure Debye temperature  $\theta_D^0$  and ambient-pressure Grüneisen parameter  $\gamma_G^0$ , which have not been determined for our system yet. To obtain  $\gamma_G^0$  we have performed the volume thermal expansion coefficient  $\alpha$  measurements, described in the next section. This allows to calculate the Grüneisen parameter at ambient conditions:<sup>40</sup>

$$\gamma_G^0 = \frac{\alpha B V_0 N_A}{C_V}, \quad (11)$$

where  $V_0$  is the primitive cell volume,  $N_A$  is the Avogadro number, and  $C_V$  is the molar constant-volume heat capacity taken as the Dulong-Petit limit of 24.94 (J K<sup>-1</sup> mol<sup>-1</sup>). The second order Grüneisen parameter is given by the following relation:<sup>43,44</sup>

$$q_0 = 1 + \delta_T - B', \quad (12)$$

TABLE I. Computed and experimental values of the Debye temperature  $\theta_D$ <sup>32,48-50</sup>, the bulk modulus  $B$ , the pressure derivate of the bulk modulus  $B'$ <sup>51</sup>, the Grüneisen parameter  $\gamma_G^0$ <sup>52</sup> and the second order Grüneisen parameter  $q_0$  [Eq. 15] at ambient conditions.

	$\theta_D$ (K)	$B$ (GPa)	$B'$	$\gamma_G^0$	$q_0$
Nb (calc)	271	163	3.52	1.55	0.14
Nb (expt.)	270-280	169	4.02	1.59	0.16
Ta (calc)	219	194	3.787	1.427	0.067
Ta (expt.)	229-258	194	3.80	1.64	0.48

where  $\delta_T$  is the so-called Grüneisen-Anderson parameter:<sup>45</sup>

$$\delta_T \equiv \frac{\partial \ln \alpha}{\partial \ln V}. \quad (13)$$

Using Dugdale and MacDonald<sup>46</sup> work, Chang et al., obtained a simple relation between  $\delta_T$  and  $\gamma_G^0$ :<sup>47</sup>

$$\delta_T = 2\gamma_G^0. \quad (14)$$

Finally, second order Grüneisen parameter may be calculated at ambient conditions as<sup>47</sup>:

$$q_0 = 1 + 2\gamma_G^0 - B'. \quad (15)$$

Bulk modulus values  $B$  and  $B'$  were determined above from the  $P(V)$  fit, thus the only parameter which remained to be determined is the power-law coefficient  $n$  from Eq.(8). Unfortunately there are no available literature data to estimate  $n$ , even for the constituent elements of TNHZT. To overcome this difficulty, first-principles phonon calculations in the pressure range of 0 - 100 GPa were performed for elemental Nb and Ta, which are the main components of our HEA and have the same bcc crystal structure. This allowed us to validate the above-described method of calculating  $\theta_D(P)$  as well as to obtain some information about the value of  $n$ .

Calculations of the phonon densities of states for Nb and Ta were performed using a QUANTUM ESPRESSO software<sup>53,54</sup>. We used projected augmented wave (PAW) pseudopotentials<sup>55,56</sup>, with the Perdew-Burke-Ernzerhof generalized gradient approximation for the exchange-correlation potential<sup>57</sup>. First, phonon densities of states  $F(\omega)$  were computed for various pressures and then the Debye temperature was calculated, based on the  $m$ -th moment of the phonon spectrum:

$$\mu_m = \int_0^{\omega_{\max}} \omega^m F(\omega) d\omega \Big/ \int_0^{\omega_{\max}} F(\omega) d\omega \quad (16)$$

$$\omega_D(m) = \left(\frac{m+3}{3}\mu_m\right)^{1/m}. \quad (17)$$

Among many available formulas for the "theoretical" Debye temperature (see, Ref.<sup>40,58</sup> for more details) we choose the one, which corresponds to the correct representation of the heat capacity for  $T > \theta_D$ , i.e.  $m = 2$ ,

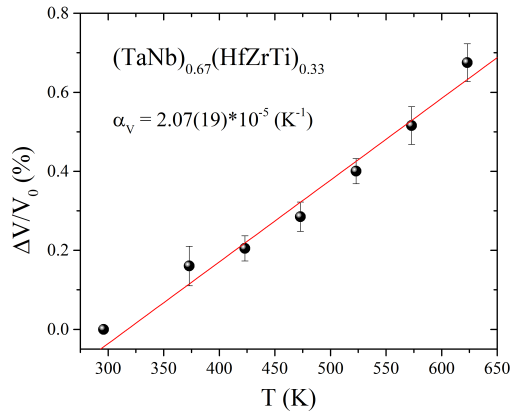


FIG. 4. Temperature dependence of a relative change of the unit cell volume. The lattice parameter was obtained by the LeBail method. A cubic  $Im\bar{3}m$  (s.g. no 229) structure was used as a starting model.

and  $k_B\theta_D = \hbar\omega_D(2)$ . However, since our materials have a simple acoustic phonon spectrum,  $\theta_D$  computed using different values of  $m$  do not change in more than 5%. It should be noted that there is no conflict between Eqs.(16)-(17) and approximation  $\langle\omega^2\rangle = \frac{1}{2}\theta_D^2$ . To avoid any confusions we explain the difference between  $\langle\omega^2\rangle$  (that enters Eq. (1)) and the second moment of the phonon DOS function in Supplemental Material<sup>34</sup>.

Computed and experimental values of the bulk modulus  $B$ , its pressure derivative  $B'$ , the Grüneisen parameter  $\gamma_G^0$ , and the second order Grüneisen parameter  $q_0$  for Nb and Ta are gathered in Table I. The second order Grüneisen parameter  $q_0$  is calculated using Eq. 15. The  $\theta_D^0$  parameter obtained from the phonon calculations and at zero pressure is 271 K for Nb and 219 K for Ta. The calculated Debye temperature of Nb remains in a very good agreement to the experimental values, which span the range of 270-280 K<sup>32,48</sup>. The  $\theta_D^0$  of Ta is slightly smaller than the literature values that range from 229 K<sup>49</sup> via 245 K,<sup>50</sup> up to 258 K<sup>32</sup>. Grüneisen model calculations of  $\theta(P)$  were performed using the computed  $\theta_D^0$  and other parameters, shown in Table I and for several values of  $n$ , ranging from 4 to 16. The values of  $\theta(P)$ , calculated directly from phonon DOS under pressure (shown in Supplemental Material<sup>34</sup>) and from the Grüneisen model for representative values of  $n$  are compared in Fig. 2 for Nb and Fig. 3 for Ta. In the case of Nb an almost perfect agreement is found. Larger deviation is seen for Ta, but still the differences between the model and first-principle calculations are smaller than 10%. It is also worth noting that our model calculations of  $\theta_D(P)$  for Ta remain in a very good agreement with the quasi-harmonic approximation calculations of Liu *et al.*<sup>39</sup>. The general observation is that the pressure dependence of  $\theta_D$  is quite well captured by the Debye-Grüneisen model, which contains only one free parameter,  $n$ . Moreover, the

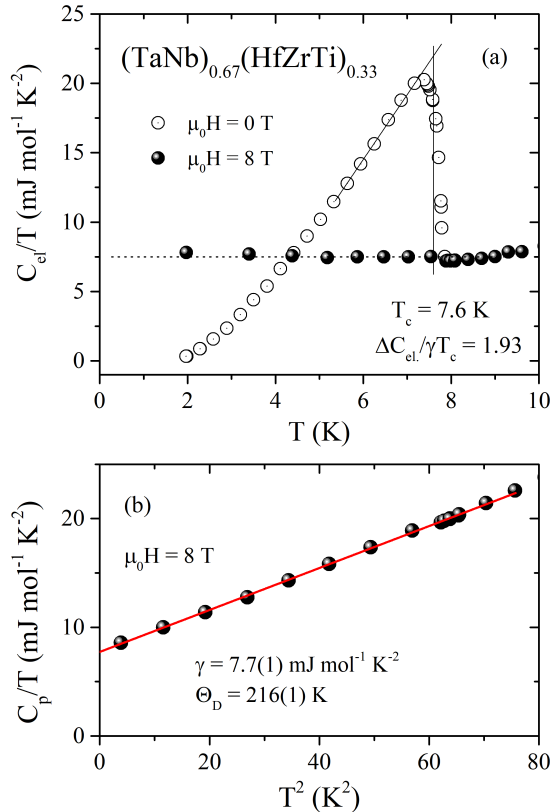


FIG. 5. Panel (a): temperature dependence of the electronic heat capacity  $C_{el}/T$  in zero (open circles) and 8 T (close circles) magnetic field. Panel (b): low temperature experimental data  $C_p/T$  vs.  $T^2$ . The solid red line is a fit by the expression  $C_p/T = \gamma + \beta T^2$ .

computed  $\theta_D(P)$  are not very sensitive to the particular choice of  $n$  due to relatively small  $q_0$  values. In the case of Nb, where the agreement is better,  $n = 16$  seems to be the best choice. Therefore, this value will be assumed in the analysis of HEA, where due to the presence of chemical disorder a phonon spectrum was not calculated.

To summarize the methodology section, electron-phonon coupling constant  $\lambda$  is calculated using Eq. (3), McMillan-Hopfield parameters are computed from band-structure results using Eq. (2), ambient-pressure values of the Debye temperature  $\theta_D^0$  and the Grüneisen parameters  $\gamma_G^0$  and  $q_0$  are taken from experiment, and the evolution of  $\theta_D$  with pressure is modelled using Eq. (9-10), where  $n = 16$  is assumed.

### III. RESULTS AND DISCUSSION

#### A. The thermal expansion and heat capacity

The  $(\text{TaNb})_{0.67}(\text{HfZrTi})_{0.33}$  as-cast sample was characterized using X-ray diffraction method (XRD). The

TABLE II. Volume thermal expansion coefficient  $\alpha_V$  ( $\text{K}^{-1}$ ), zero-pressure Grüneisen parameter (dimensionless) and the bulk modulus  $B$  (GPa) of TNHZT, determined in this work, compared to several refractory HEAs<sup>59, 60</sup>.

	$\alpha_V$	$\gamma_G^0$	B
TNHZT (this work)	2.07	1.62	177.4
TiZrHfVNb	3.60	1.83	79.0
TiZrVNb	3.34	1.65	84.2
TiZrVNbMo	3.32	2.19	125.0
NbTaMoW	2.67	2.40	162.5
NbHfZrTi	2.30	-	88.3

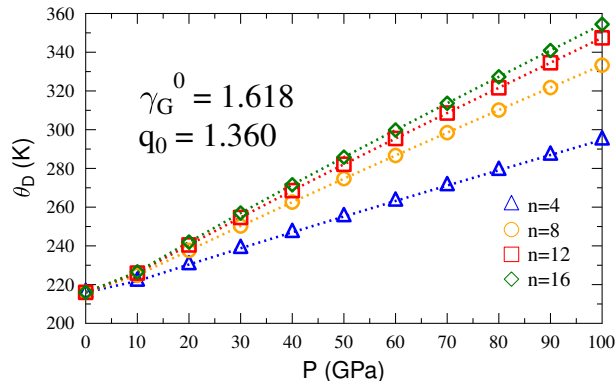


FIG. 6. Simulated pressure dependence of  $\theta_D$  of TNHZT.

measurement was first performed at room temperature and then at temperatures from 100°C up to 400°C with a step of 50 deg. The XRD pattern is shown in the Supplemental Material<sup>34</sup> and contains only sharp  $\text{Al}_2\text{O}_3$  (holder) reflections and reflections that were indexed with an I-centered cubic phase. A cubic lattice parameter for TNHZT was refined using the LeBail method and High-Score software. A relative change of a unit cell volume ( $\Delta V/V_0$ ) vs. temperature is presented in Figure 4. The volumetric thermal expansion coefficient was found to be  $\alpha = 2.07(19) \times 10^{-5} \text{ K}^{-1}$  and is comparable to those obtained for the constituting metals [for which it changes from 17.1 (Zr) to 27 (Ti), given in ( $10^{-5} \text{ K}^{-1}$ )].

The temperature dependence of the electronic heat capacity,  $C_{\text{el}}/T$  of  $(\text{TaNb})_{0.67}(\text{HfZrTi})_{0.33}$  is presented in Fig. 5(a). The experimental data were collected under zero (open circles) and applied magnetic field (close circles). The  $C_{\text{el}}$  was obtained from the relation  $C_p = C_{\text{el}} + C_{\text{ph}}$ , where  $C_{\text{ph}} = \beta T^3$  is the low temperature ( $T < \theta_D/50$ ) phonon contribution. In order to obtain  $\beta$ , the heat capacity in the normal state was measured and the data are presented in panel (b), plotted as  $C_p/T$  vs.  $T^2$ . In the normal state  $C_p$  can be analyzed by  $C_p = \gamma T + \beta T^3$ , where  $\gamma T$  is the contribution from the conduction electrons. The fit is represented by a solid red line with the fitting parameters:  $\gamma = 7.7(1) \text{ mJ mol}^{-1} \text{ K}^{-2}$  and  $\beta = 0.193(2) \text{ mJ mol}^{-1} \text{ K}^{-4}$ . Then, we

can calculate the Debye temperature from the relation:  $\theta_D = [(12\pi R)/(5\beta)]^{1/3}$ , where  $R$  is the gas constant. Both the Sommerfeld parameter and Debye temperature  $\theta_D = 216(1) \text{ K}$  are in good agreement with those reported previously<sup>15</sup> ( $\gamma = 7.97 \text{ mJ mol}^{-1} \text{ K}^{-2}$ ,  $\theta_D = 225 \text{ K}$ ). The sharp anomaly at  $T_c = 7.6 \text{ K}$ , seen in the  $C_{\text{el}}/T$  confirms a bulk nature of superconductivity in the studied sample. A normalized jump of the specific heat  $\Delta C/\gamma T_c = 1.93$  is comparable to that reported in Ref. 15. The estimated value exceeds the one expected for weak-coupling BCS superconductors  $\Delta C/\gamma T_c = 1.43$ , indicating that  $(\text{TaNb})_{0.67}(\text{HfZrTi})_{0.33}$  is an intermediate- or strong-coupling superconductor.

## B. The Debye temperature under pressure

Evolution of the Debye temperature with pressure, needed to calculate  $\lambda$  in our approach, was simulated according to the model described above. The ambient-pressure Grüneisen parameter  $\gamma_G^0$  was calculated using Eq. 11. The lattice thermal expansion coefficient and unit cell volume have been measured experimentally and heat capacity was approximated by the Dulong-Petit law. The parameters  $B = 177 \text{ GPa}$  and  $B' = 2.87$  were determined from the Birch-Murnaghan equation of state<sup>6</sup>. Values of those parameters are gathered in Table II, along with a data reported for similar alloys<sup>59</sup>. The lattice thermal expansion coefficient of TNHZT is relatively low and it is accompanied by a large bulk modulus. The obtained value of the Grüneisen parameter  $\gamma_G^0 = 1.62$  is similar to that found for the other listed alloys. Using Eq.(15), the second-order Grüneisen parameter  $q_0 = 1.36$  is obtained. It is larger than  $q_0$  of Nb and Ta, which is a direct consequence of smaller  $B'$  observed in TNHZT. Unfortunately, there are no other reported values of  $q_0$  (to the best of our knowledge) among HEAs to compare with. The calculated evolution of  $\theta_D$  under pressure are shown in Fig. 6 for different values of  $n$ . For larger  $n$ ,  $\theta_D(P)$  becomes insensitive to choice of  $n$  and we assume  $n = 16$  in further analysis. It also gave the closest results to the first-principles modeling and quasi-harmonic calculations for Nb and Ta, as described above. Finally,  $\theta_D$  increases almost linearly with pressure and reaches 360 K at  $P = 100 \text{ GPa}$ .

## C. Electronic structure

Figure 7 presents total and atomic densities of states of TNHZT, calculated under various pressures. In  $(\text{TaNb})_{67}(\text{HfZrTi})_{33}$  and at ambient conditions, the Fermi level is located in the DOS peak, similarly to the first superconducting HEA,  $\text{Ta}_{34}\text{Nb}_{33}\text{Hf}_8\text{Zr}_{14}\text{Ti}_{11}$ <sup>10</sup>. Main contributions to the total DOS originate from the  $d$ -shells of all constituent atoms ( $3d$  for Ti,  $4d$  for Zr and Nb, and  $5d$  for Hf and Ta). As the pressure increases, DOS strongly decreases. It is mainly due to enhanced

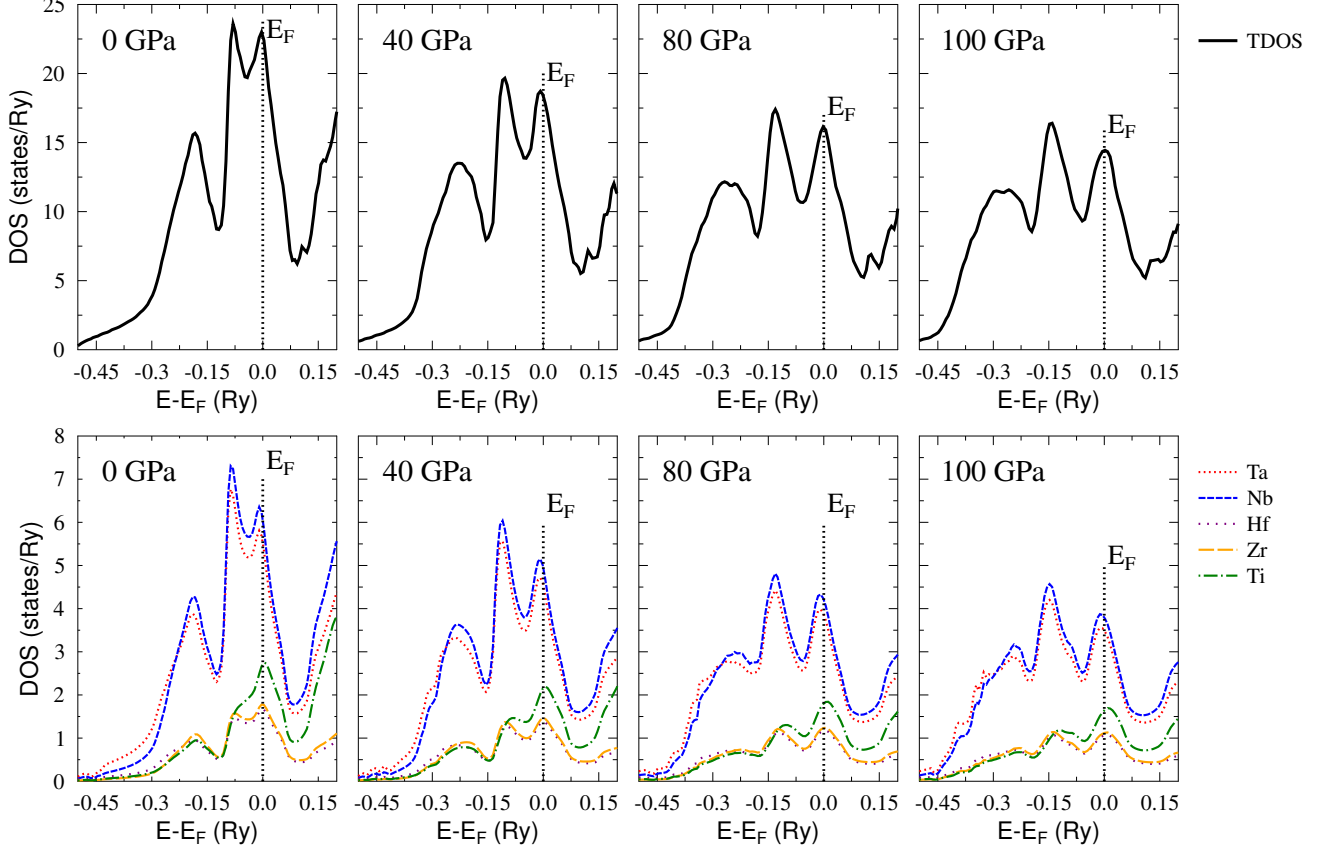


FIG. 7. Total and atomic densities of states of TNHZT alloy, calculated under various pressures in the range of 0 to 100 GPa. Solid black line represents the total DOS. Atomic densities of states are plotted with colors and weighted over its concentrations.

TABLE III. Electronic properties of  $(\text{TaNb})_{67}(\text{HfZrTi})_{33}$ .  $M_i$  is given in u,  $c_i$  in %,  $N(E_F)$  in  $\text{Ry}^{-1}$ ,  $\eta$  in  $\text{mRy}/a_B^2$ .

	$c_i$	$M_i$	$N(E_F)$	$\eta_i$	$\eta_{sp}$	$\eta_{pd}$	$\eta_{df}$
Ta	33.5	181	16.54	151.79	0.83	49.08	101.90
Nb	33.5	93	18.10	157.09	4.46	53.19	99.45
Hf	11	179	15.20	156.30	1.58	66.16	88.60
Zr	11	91	16.21	165.01	6.55	73.16	85.28
Ti	11	41	24.78	119.17	4.80	43.56	70.80

hybridization and decrease of the unit cell volume. Furthermore, applied pressure increases separation of the two highest DOS peaks (one located at the Fermi level and the second one below  $E_F$ ) and shifts electronic states to a lower energy range (i.e. increases the bandwidth). In addition, a shift of electronic states causes a gradual decrease of the third DOS maximum, lying in the lowest energy range. Atom with the largest contribution to the total DOS at  $E_F$  is Ti (see also Table III) for both ambient and elevated pressure conditions. Fig. 8 shows the gradual decrease of the  $N(E_F)$  value with pressure, from about  $22.5 \text{ Ry}^{-1}$  to  $14.5 \text{ Ry}^{-1}$  at 100 GPa. The ambient-pressure value corresponds to the non-interacting Som-

merfeld parameter  $\gamma_0 = 3.9 \text{ mJ mol}^{-1} \text{ K}^{-2}$ . Comparison to the experimental value of  $\gamma = 7.7(1) \text{ mJ mol}^{-1} \text{ K}^{-2}$  gives the electron-phonon enhancement parameter

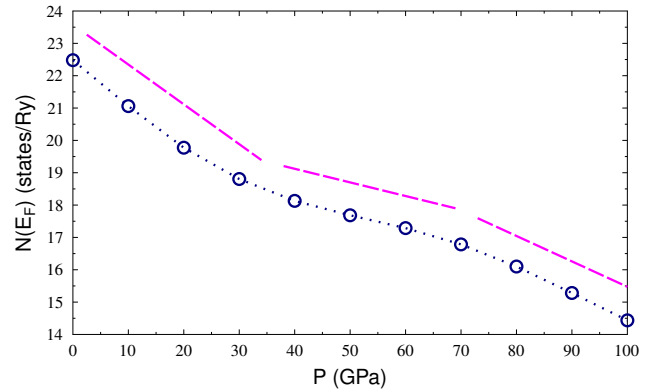


FIG. 8. Variation of the density of states at the Fermi level under hydrostatic pressure from 0 to 100 GPa. Dashed lines are the linear trend lines, described in the text.

$\lambda = \gamma/\gamma_0 - 1 = 0.97$ , which is very close to the value obtained for  $\text{Ta}_{34}\text{Nb}_{33}\text{Hf}_8\text{Zr}_{14}\text{Ti}_{11}$ <sup>10</sup>.

In the  $N(E_F)$  versus  $P$  relation (Fig. 8) we can distinguish three regions. At first,  $N(E_F)$  quickly decreases with a slope of  $-0.123 \text{ Ry}^{-1}/\text{GPa}$  up to 40 GPa. Above 40 GPa, the decrease becomes slower ( $-0.042 \text{ Ry}^{-1}/\text{GPa}$ ), and then, above 70 GPa, the slope becomes more negative, reaching  $-0.079 \text{ Ry}^{-1}/\text{GPa}$ . Interestingly, this evolution is correlated with the observed modifications of  $T_c$  under pressure, where  $T_c$  increases monotonically up to 10 K at around 50 GPa. Above that pressure, the transition temperature, remains practically constant. To analyze this trend of  $N(E_F)$ , electronic dispersion relations were computed using the complex energy band technique, attainable in the KKR-CPA formalism<sup>61–63</sup>. In this method, the real part of electron energy shows the band center, whereas the imaginary part describes the band smearing effects caused by a chemical disorder. A bandwidth is related to the electronic life time that is finite due to the presence of the disorder-induced electron scattering,  $\tau = \hbar/2\text{Im}(E)$ . As we have shown in Ref.<sup>10</sup> in the case of  $\text{Ta}_{34}\text{Nb}_{33}\text{Hf}_8\text{Zr}_{14}\text{Ti}_{11}$ , electronic bands were rather sharp with small smearing effect, in spite of the high level of disorder. As seen in Fig. 9 the same situation is found here, especially near  $E_F$ , where the small imaginary part of energy gives  $\tau \sim 0.5 - 1 \times 10^{-14}$  s. Also, the smearing near  $E_F$  does not change much under pressure, although it increases for the lower-lying states.

On the whole, upon external pressure both empty and occupied electronic bands move towards  $E_F$ . Interesting evolution is found in the  $N - \Gamma$  direction, where the local minimum of one of the bands is near  $E_F$  (peak in DOS is associated with this band). As shown in Fig. 10, above 50 GPa this band comes very close to  $E_F$  and its center actually crosses  $E_F$  at around  $\sim 70$  GPa, leading to a Lifshitz transition<sup>64</sup> (change of the Fermi surface topology). This topological transition is also visualized in Fig. 11, where  $k_x - k_y$  cross-sections of the Fermi surface are plotted for 0, 50 and 100 GPa. The appearance of an additional band at the Fermi level is correlated with the slowing down of the decrease in  $N(E_F)$  around 40 GPa, as discussed above. The fact that the band is actually blurred by the disorder leads to smearing of this transition and the band starts to contribute to DOS at lower pressures.

What is worth noting, two transitions in topology of electronic states under pressure were reported theoretically<sup>65</sup> for pure Nb; one slight change in the Fermi surface shape at 5–6 GPa and more prominent one around 60 GPa, connected to similar shift in electronic band in  $N - \Gamma$ . In an earlier experiment<sup>66</sup>,  $T_c$  of Nb was reported to show anomalies around these pressures (increase by 0.7 K and decrease by 1 K, respectively) and changes in the topology of the Fermi surfaces were given as an explanation for these anomalies in Ref.<sup>65</sup>. However, in another theoretical work<sup>67</sup>, where relativistic full potential LMTO calculations were presented, only the second transition was observed, at around 60 GPa of

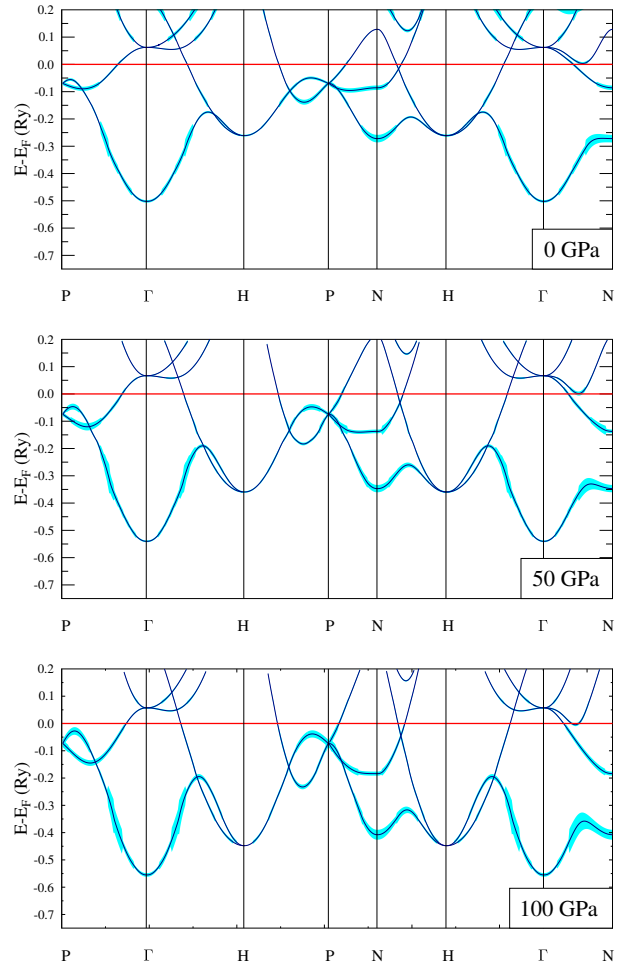


FIG. 9. Electronic dispersion relations for  $P = 0, 50$  and  $100$  GPa. Shading describes the band smearing and corresponds to the imaginary part of the complex energy.

hydrostatic pressure. The first anomaly in  $T_c$ , reported in Ref.<sup>66</sup> was ascribed to the presence of non-uniform pressure conditions or polycrystalline sample effects. In our case the  $T_c$  increases monotonically up to about 50 GPa and remains practically constant above that pressure. This trend may be correlated to the observed Lifshitz transition, which is additionally smeared by the disorder effects.

#### D. Electron-phonon coupling

Values of the ambient-pressure McMillan-Hopfield parameters are gathered in Table III. Titanium, despite highest  $N(E_F)$  has the lowest contribution to the electronic part of the EPC, while the highest belongs to Zirconium. Interestingly, Zr atoms also present almost equal contribution to  $\eta$  from the  $p-d$  and  $d-f$  scattering channels. For other constituent atoms,  $d-f$  scattering channel

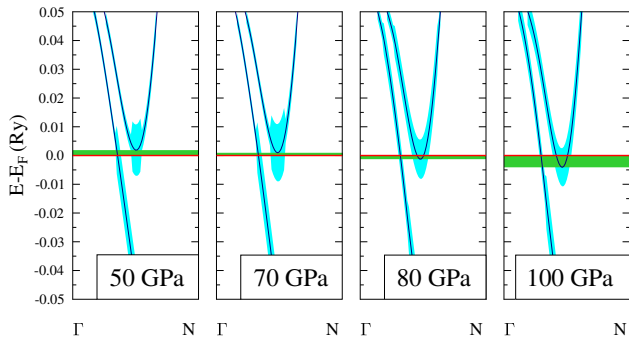


FIG. 10. Electronic dispersion relations near  $E_F$  in  $\Gamma - N$  direction, showing the Lifshitz transition. The distance between the center of the band and the Fermi level is marked in green. Shading describes the band smearing and corresponds to the imaginary part of the complex band energy.

gives the largest contribution to  $\eta$  and it is typical for transition metal elements. To have a reference point,  $\eta$  for pure Nb is about  $165 \text{ mRy}/a_B^2$ <sup>35</sup>, and calculated  $\eta_i$  are slightly smaller than for  $\text{Ta}_{34}\text{Nb}_{33}\text{Hf}_8\text{Zr}_{14}\text{Ti}_{11}$ <sup>10</sup>. Using Eq. 3, the calculated  $\eta_i$  and the experimental Debye temperature  $\theta_D = 216 \text{ K}$ , we get the ambient pressure electron-phonon coupling constant  $\lambda = 1.1$ . **This value is** in close agreement with 0.97 determined above from the renormalization of the Sommerfeld coefficient  $\gamma$ .

Evolution of the McMillan-Hopfield parameters with pressure is shown in Fig. 12; a concentration-weighted sum in the top panel and  $\eta_i$  per atom in the bottom panel. In both cases the evolution is very smooth, with gradual increase in  $\eta$ . What can be noticed in Fig. 12(a) is the slight change of slope of the curve, above 40-50 GPa, which resembles the one seen in  $N(E_F)$  variation in Fig. 8. Nevertheless, the evolution of  $\eta$  is rather typical, as  $\eta$  generally increases with pressure<sup>29,68,69</sup>. Less obvious is the change of the distribution of  $\eta$  among the  $s - p - d - f$  scattering channels, which is plotted in Fig. 13. For the group 4 elements, i.e. Hf, Zr, Ti, a change of the dominating scattering channel to  $p - d$  at high pressures is observed. Such a **behavior** is not observed for Ta and Nb atoms, **although** values of  $\eta_{pd}$  and  $\eta_{df}$  become close to each other. **The increase in  $\eta_i$  is related to the increase in the matrix elements in Eq.(2), which we additionally plotted in Supplemental Material<sup>34</sup>.**

The pressure evolution of  $\lambda$ , obtained **based** on computed  $\eta_i(P)$  parameters (Fig. 12), simulated evolution of Debye temperature  $\theta_D(P)$  (Fig. 6) and Eq.3 is shown in Fig. 14. After an initial increase, we observe a general decrease in  $\lambda$ . This is due to the fact that the evolution of the electron-phonon coupling constant  $\lambda$  with pressure is the **result** of two competitive effects; an increase of the McMillan-Hopfield  $\eta$  and increase of the phonon frequencies  $\omega$ , here represented by the Debye temperature  $\theta_D$ .

Taking the derivative of  $\ln \lambda$  from Eq.(3) we get:

$$\frac{d \ln \lambda}{dP} = -\frac{1}{\tilde{B}} \left( \frac{d \ln \eta}{d \ln V} + 2\gamma_G \right), \quad (18)$$

where  $\eta = \sum_i c_i \eta_i$  and  $\gamma_G = -\frac{d \ln \theta_D}{d \ln V}$ . **The** simplified pressure-volume equation of state  $V = V_0 \exp(-P/\tilde{B})$  was used to convert the pressure derivative into the volume one. The value of such-defined  $\tilde{B}$  "bulk modulus" is of no importance here for the qualitative discussion. The McMillan-Hopfield parameters increase when the unit cell volume decreases, thus  $\frac{d \ln \eta}{d \ln V}$  is negative<sup>29,68,69</sup> and its value is usually between -1.0 and -3.0. From the equation above, we **can** see that  $\lambda(P)$  would be an increasing function of pressure for the case where  $-\frac{d \ln \eta}{d \ln V} > 2\gamma_G$ . In our case  $2\gamma_G \simeq 3.0$  and  $-\frac{d \ln \eta}{d \ln V} < 3.0$  for all pressures above 20 GPa, **and, therefore**, a decreasing  $\lambda(P)$  function is expected. **This is exactly** what we can see in Fig. 14, where  $\lambda$  **decreases** with pressure above 10 GPa. Only at 10 GPa, due to the strong increase of  $\eta$ , an increase of calculated  $\lambda$  is observed, since the condition  $-\frac{d \ln \eta}{d \ln V} > 2\gamma_G$  is fulfilled. At ambient conditions we have  $\lambda = 1.10$ . **It raises to  $\lambda \simeq 1.15$  at 10 GPa and then gradually decreases for larger pressures, reaching 0.88 at 100 GPa.**

Finally, the superconducting critical temperature may be calculated using McMillan formula<sup>32</sup>:

$$T_c = \frac{\theta_D}{1.45} \exp \left[ -\frac{1.04(1 + \lambda)}{\lambda - \mu^*(1 + 0.62\lambda)} \right]. \quad (19)$$

The last parameter, which has to be determined is the Coulomb pseudopotential parameter,  $\mu^*$ . In zero pressure, the most-commonly used value of 0.13 would lead to an overestimated  $T_c = 12.5 \text{ K}$ . To get the experimental zero pressure  $T_c = 7.7 \text{ K}$  one has to **use**  $\mu^* = 0.215$ . Similar value was used for pure Nb to reproduce the experimental critical temperature **based on the calculated** Eliashberg function<sup>67,70</sup>. Even larger values of  $\mu^*$  were postulated for other materials **such as**  $\text{Nb}_3\text{Ge}$  ( $\mu^* = 0.24$ )<sup>71</sup>, V ( $\mu^* = 0.3$ )<sup>70</sup> or  $\text{MgCNi}_3$  ( $\mu^* = 0.29$ )<sup>72</sup>. Thus, to explore the variation of  $T_c$  with pressure we assume  $\mu^*(0) = 0.215$ . For  $P > 0$ ,  $T_c(P)$  was calculated in two ways. First,  $\mu^* = 0.215$  was kept constant in the whole pressure range. Next,  $\mu^*(P)$  dependence was assumed to originate from the pressure dependence of  $N(E_F)$  and calculated using the Benneman and Garland formula<sup>73</sup>:

$$\mu^* = \frac{AN(E_F)}{1 + N(E_F)}, \quad (20)$$

where  $N(E_F)$  is in  $\text{eV}^{-1}$  per atom. Originally, Benneman and Garland set  $A = 0.26$  to get  $\mu^* = 0.13$  for the typical case of a metal with  $N(E_F) = 1 \text{ eV}^{-1}$  per atom. **Therefore**, in our case where  $N(E_F) = 1.65 \text{ eV}^{-1}$  for  $P = 0$  and postulated  $\mu^*(0) = 0.215$  we use  $A = 0.345$ , and simulate  $\mu^*(P)$  dependence according to  $N(E_F)$  variation with pressure (Fig. 8) by using Eq.(20). Fig. 15 shows the  $\mu^*(P)$  dependence **that** decreases smoothly with pressure

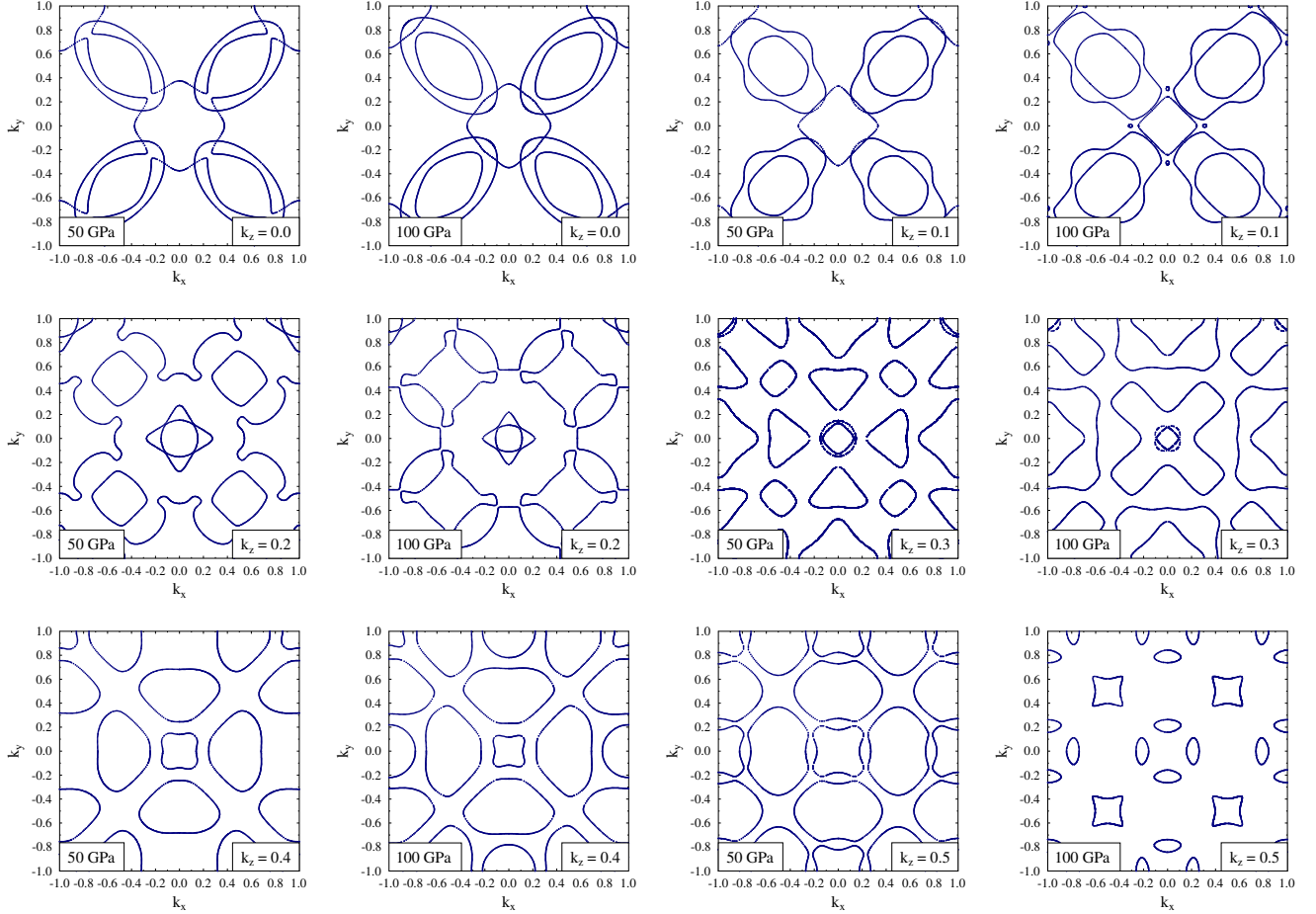


FIG. 11. Cross sections of Fermi surface, calculated under pressures of 50 and 100 GPa.  $k$  is given in  $2\pi/a$ .

and drops to 0.17 at 100 GPa. Finally, Fig. 16 shows the computed critical temperature  $T_c(P)$ , where  $T_c$  for the "standard"  $\mu^* = 0.13$  as also included.

In general, under the assumption of relatively large  $\mu^*(0) = 0.215$ , our calculations quite well predict the variation of  $T_c$  with pressure (but only when variable  $\mu^*(P)$  is used). In spite of the decrease in the computed  $\lambda$  above 10 GPa,  $T_c$  increases up to 40 - 50 GPa and then remains almost constant up to 100 GPa, just like it is observed in the experiment. This counter-intuitive observation shows the delicate balance between  $T_c$ ,  $\theta_D$ , and  $\lambda$ , since an increase in  $\theta_D$  leads to a quadratic increase in the denominator of Eq.(3) (tendency to decrease  $\lambda$ ) and linear increase of  $T_c$  via the multiplier in McMillan's Eq.(19). In stabilization of  $T_c$  above 40 GPa, the decrease of  $\mu^*$ , which results from the decrease in  $N(E_F)$  occurs to be equally important, since for the constant  $\mu^*$  decrease in  $T_c$  is predicted by the theoretical calculations. This shows that up to a studied pressure of 100 GPa, the evolution of  $T_c$  with pressure in  $(\text{TaNb})_{0.67}(\text{HfZrTi})_{0.33}$  can be explained by the classical electron-phonon mechanism. This is surprisingly well captured by a combination

of coherent potential approximation, rigid muffin tin approximation, and "averaged" phonon spectrum. Thus, structural local short-range ordering effects or local distortions of the crystal structure that are likely present in the studied samples, seem not to have a large impact on superconductivity. This may be understood as the superconducting coherence length being typically much larger than the structural anomalies' length scale. Based on the upper critical field data from Ref.<sup>15</sup> ( $\mu_0 H_{c2} = 7.75$  T) the superconducting coherence length may be estimated as 65 Å. This is roughly 20 times the lattice parameter of the system. On this length scale the possible local crystal structure distortions or chemical inhomogeneities are averaged out, and therefore an effective medium theory that we apply here, works well.

#### IV. SUMMARY

In summary, we have studied pressure effects of the electronic structure, electron-phonon interaction, and superconductivity of the high entropy alloy

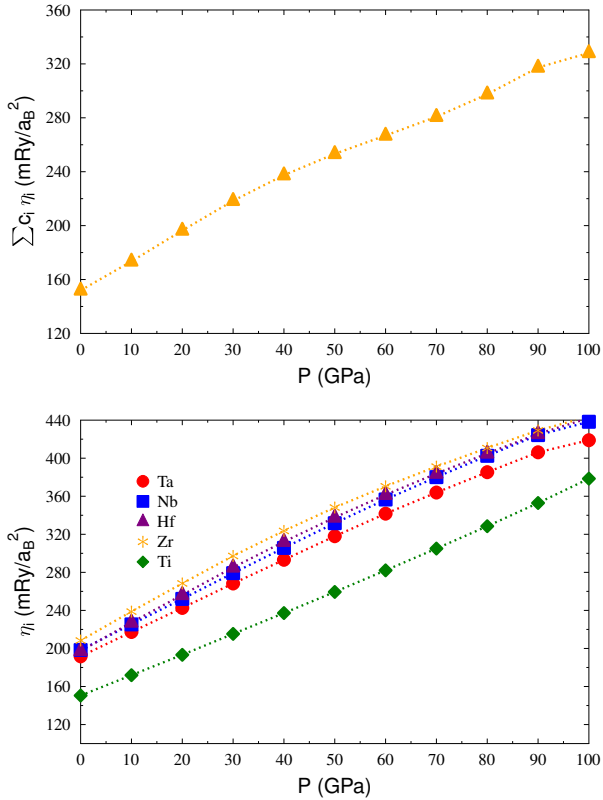


FIG. 12. Pressure evolution of the McMillan-Hopfield parameters: concentration-weighted sum (top) and  $\eta_i$  per atom (bottom).

$(\text{TaNb})_{0.67}(\text{HfZrTi})_{0.33}$  in a pressure range from 0 to 100 GPa. With increasing pressure the total density of states at the Fermi level  $N(E_F)$  gradually decreases. Lifshitz transition is observed around 70 GPa when one of the bands starts crossing the Fermi level. Due to disorder-induced band smearing effects, however, the transition is

not sharp, since these bands contribute to  $N(E_F)$  also at lower pressures (even below 50 GPa). As in the experimental studies,  $T_c(P)$  changes the slope above 50 GPa and this effect may be correlated with the calculated band structure evolution and the Lifshitz transition. The effects of pressure on the lattice dynamics were simulated using the Debye-Grüneisen model, where  $\gamma_G$  parameter was additionally determined. The calculated McMillan-Hopfield parameters increase with pressure but due to concurrent effect of the lattice stiffening and increase of the Debye temperature, the electron-phonon coupling parameter  $\lambda$  decreases above 10 GPa. In spite of this, the calculated superconducting  $T_c$  increases up to 40 - 50 GPa and later is stabilized at the larger value of  $\lambda$  than observed at the ambient conditions. This non-decreasing  $T_c$  results from the increase of the Debye temperature and decrease of  $N(E_F)$ , which is caused by the monotonic decrease of the Coulomb pseudopotential parameter  $\mu^*$ . Our results are in good agreement with the experimental trend and shows that up to a studied pressure of 100 GPa the evolution of  $T_c$  with pressure in  $(\text{TaNb})_{0.67}(\text{HfZrTi})_{0.33}$  can be well explained by the classical electron-phonon mechanism. This implies that the electronic structure of the system is well described by the coherent potential approximation. An excellent additional test of our theoretical results would be a measurement of the electronic heat capacity under pressure, which would allow verification of the observed decrease in both  $N(E_F)$  and  $\lambda$ .

## V. ACKNOWLEDGMENTS

KJ and BW were supported by the National Science Center (Poland), grant No. 2017/26/E/ST3/00119. K. Gofryk acknowledges support from DOE’s Early Career Research Program. JT was supported by the AGH-UST statutory tasks No. 11.11.220.01/5 within subsidy of the Ministry of Science and Higher Education.

\* wiendlocha@fis.agh.edu.pl

- <sup>1</sup> A. P. Drozdov, M. I. Erements, I. A. Troyan, V. Ksenofontov, and S. I. Shylin, “Conventional superconductivity at 203 kelvin at high pressures in the sulfur hydride system,” *Nature (London)* **525**, 73–76 (2015).
- <sup>2</sup> A. P. Drozdov, P. P. Kong, V. S. Minkov, S. P. Besedin, M. A. Kuzovnikov, S. Mozaffari, L. Balicas, F. F. Balakirev, D. E. Graf, V. B. Prakapenka, E. Greenberg, D. A. Knyazev, M. Tkacz, and M. I. Erements, “Superconductivity at 250 K in lanthanum hydride under high pressures,” *Nature (London)* **569**, 528–531 (2019).
- <sup>3</sup> R. Szcześniak and A. P. Durajski, “Superconductivity well above room temperature in compressed  $\text{MgH}_6$ ,” *Frontiers of Physics* **11**, 117406 (2016).
- <sup>4</sup> R. Szcześniak and A. P. Durajski, “Unusual sulfur isotope effect and extremely high critical temperature in  $\text{H}_3\text{S}$  su-

- perconductor,” *Scientific Reports* **8**, 6037 (2018).
- <sup>5</sup> Jing Guo, Gongchang Lin, Shu Cai, Chuanying Xi, Changjin Zhang, Wanshuo Sun, Qiuliang Wang, Ke Yang, Aiguo Li, Qi Wu, Yuheng Zhang, Tao Xiang, Robert Joseph Cava, and Liling Sun, “Record-High Superconductivity in Niobium–Titanium Alloy,” *Advanced Materials* **31**, 1807240 (2019), <https://onlinelibrary.wiley.com/doi/pdf/10.1002/adma.201807240>.
- <sup>6</sup> Jing Guo, Honghong Wang, Fabian von Rohr, Zhe Wang, Shu Cai, Yazhou Zhou, Ke Yang, Aiguo Li, Sheng Jiang, Qi Wu, Robert J. Cava, and Liling Sun, “Robust zero resistance in a superconducting high-entropy alloy at pressures up to 190 GPa,” *Proceedings of the National Academy of Sciences* **114**, 13144–13147 (2017), <https://www.pnas.org/content/114/50/13144.full.pdf>.

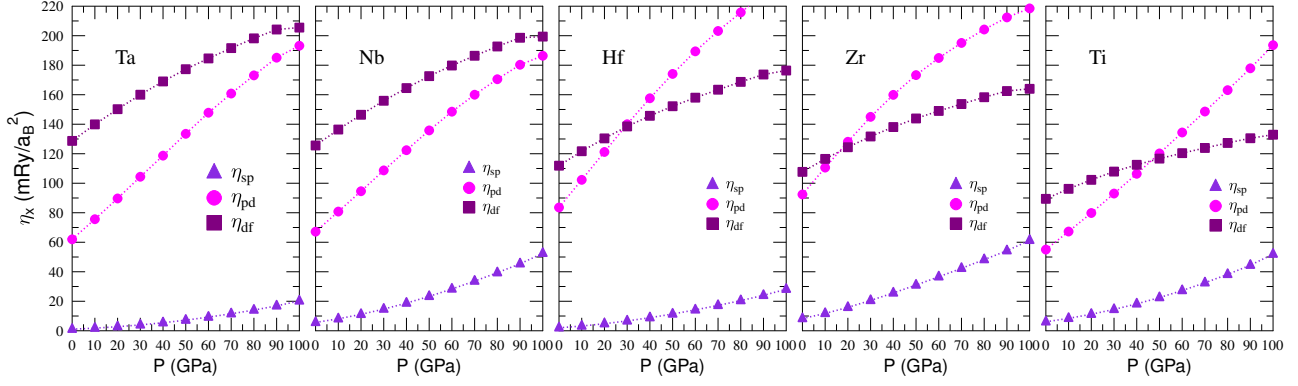


FIG. 13. Evolution of the McMillan-Hopfield parameters of each of the atom, decomposed over the  $l \rightarrow l+1$  scattering channels.

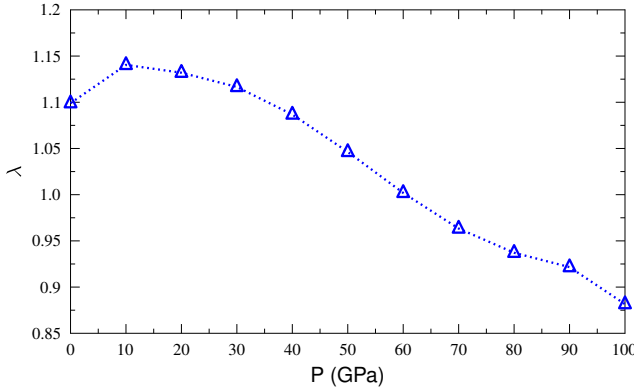


FIG. 14. Calculated evolution of the electron-phonon coupling parameter  $\lambda$  with pressure.

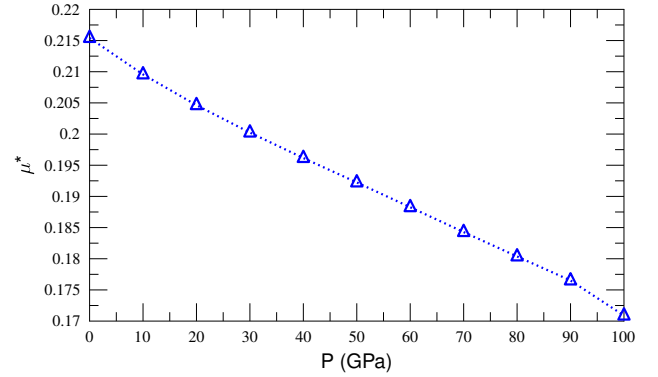


FIG. 15. Variation of the Coulomb pseudopotential parameter  $\mu^*$  with pressure, calculated using Eq.(20) and  $N(E_F)$  as in Fig. 8.

- <sup>7</sup> J.-W. Yeh, S.-K. Chen, S.-J. Lin, J.-Y. Gan, T.-S. Chin, T.-T. Shun, C.-H. Tsau, and S.-Y. Chang, “Nanostructured High-Entropy Alloys with Multiple Principal Elements: Novel Alloy Design Concepts and Outcomes,” *Advanced Engineering Materials* **6**, 299–303 (2004).
- <sup>8</sup> Jien Wei Yeh, Yu Liang Chen, Su Jien Lin, and Swe Kai Chen, “High-Entropy Alloys - A New Era of Exploitation,” in *Advanced Structural Materials III*, Materials Science Forum, Vol. 560 (Trans Tech Publications, 2007) pp. 1–9.
- <sup>9</sup> P. Koželj, S. Vrtnik, A. Jelen, S. Jazbec, Z. Jagličić, S. Maiti, M. Feuerbacher, W. Steurer, and J. Dolinšek, “Discovery of a Superconducting High-Entropy Alloy,” *Phys. Rev. Lett.* **113**, 107001 (2014).
- <sup>10</sup> K. Jasiewicz, B. Wiendlocha, P. Korbeń, S. Kaprzyk, and J. Tobola, “Superconductivity of  $\text{Ta}_{34}\text{Nb}_{33}\text{Hf}_8\text{Zr}_{14}\text{Ti}_{11}$  high entropy alloy from first principles calculations,” *Physica Status Solidi (RRL) - Rapid Research Letters* **10**, 415–419 (2016).
- <sup>11</sup> Ryota Sogabe, Yosuke Goto, and Yoshikazu Mizuguchi, “Superconductivity in  $\text{REO}_{0.5}\text{F}_{0.5}\text{BiS}_2$  with high-entropy-alloy-type blocking layers,” *Applied Physics Express* **11**, 053102 (2018).
- <sup>12</sup> Karoline Stolze, Jing Tao, Fabian O. von Rohr, Tai Kong, and Robert J. Cava, “Sc-Zr-Nb-Rh-Pd

- and Sc-Zr-Nb-Ta-Rh-Pd High-Entropy Alloy Superconductors on a CsCl-Type Lattice,” *Chemistry of Materials* **30**, 906–914 (2018), <https://doi.org/10.1021/acs.chemmater.7b04578>.
- <sup>13</sup> Karoline Stolze, F. Alex Cevallos, Tai Kong, and Robert J. Cava, “High-entropy alloy superconductors on an  $\sigma$ -Mn lattice,” *J. Mater. Chem. C* **6**, 10441–10449 (2018).
- <sup>14</sup> Fabian O. von Rohr and Robert J. Cava, “Isoelectronic substitutions and aluminium alloying in the Ta-Nb-Hf-Zr-Ti high-entropy alloy superconductor,” *Phys. Rev. Materials* **2**, 034801 (2018).
- <sup>15</sup> Fabian von Rohr, Michał J. Winiarski, Jing Tao, Tomasz Klimczuk, and Robert Joseph Cava, “Effect of electron count and chemical complexity in the Ta-Nb-Hf-Zr-Ti high-entropy alloy superconductor,” *Proceedings of the National Academy of Sciences* **113**, E7144–E7150 (2016), <https://www.pnas.org/content/113/46/E7144.full.pdf>.
- <sup>16</sup> T Stopa, S Kaprzyk, and J Tobola, “Linear aspects of the korringa-kohn-rostoker formalism,” *Journal of Physics: Condensed Matter* **16**, 4921–4933 (2004).
- <sup>17</sup> S. Kaprzyk and A. Bansil, “Green’s function and a generalized lloyd formula for the density of states in disordered muffin-tin alloys,” *Phys. Rev. B* **42**, 7358–7362 (1990).

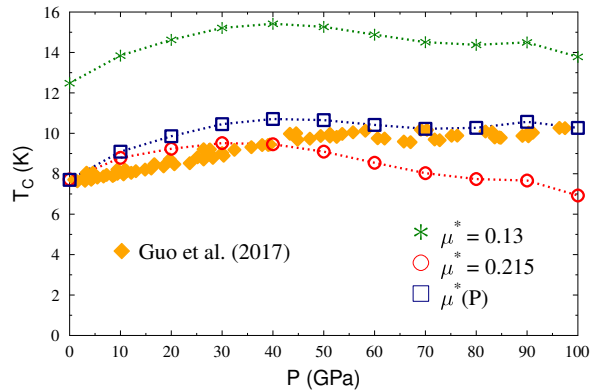


FIG. 16. Calculated pressure dependence of  $T_c$  of  $(\text{TaNb})_{0.67}(\text{HfZrTi})_{0.33}$  for two constant values of  $\mu^* = 0.13$  and  $\mu^* = 0.215$ , variable  $\mu^*(P)$  (see, Fig 15) and compared to experiment<sup>6</sup>.

<sup>18</sup> A. Bansil, S. Kaprzyk, P. E. Mijnaerends, and J. Tobola, “Electronic structure and magnetism of  $\text{Fe}_{3-x}\text{V}_x\text{X}$  ( $X = \text{Si, Ga, and Al}$ ) alloys by the KKR-CPA method,” *Phys. Rev. B* **60**, 13396–13412 (1999).

<sup>19</sup> Paul Soven, “Coherent-potential model of substitutional disordered alloys,” *Phys. Rev.* **156**, 809–813 (1967).

<sup>20</sup> G. D. Gaspari and B. L. Gyorffy, “Electron-Phonon Interactions,  $d$  Resonances, and Superconductivity in Transition Metals,” *Phys. Rev. Lett.* **28**, 801–805 (1972).

<sup>21</sup> John P. Perdew and Yue Wang, “Accurate and simple analytic representation of the electron-gas correlation energy,” *Phys. Rev. B* **45**, 13244–13249 (1992).

<sup>22</sup> K. Jasiewicz, J. Cieslak, S. Kaprzyk, and J. Tobola, “Relative crystal stability of alxfenircrco high entropy alloys from xrd analysis and formation energy calculation,” *Journal of Alloys and Compounds* **648**, 307 – 312 (2015).

<sup>23</sup> K. Jin, B. C. Sales, G. M. Stocks, G. D. Samolyuk, M. Daene, W. J. Weber, Y. Zhang, and H. Bei, “Tailoring the physical properties of ni-based single-phase equiatomic alloys by modifying the chemical complexity,” *Scientific Reports* **6** (2016), 10.1038/srep20159.

<sup>24</sup> M Calvo-Dahlborg, J Cornide, J Tobola, D Nguyen-Manh, J S Wróbel, J Juraszek, S Jouen, and U Dahlborg, “Interplay of electronic, structural and magnetic properties as the driving feature of high-entropy  $\text{CoCrFeNiPd}$  alloys,” *Journal of Physics D: Applied Physics* **50**, 185002 (2017).

<sup>25</sup> K. Jasiewicz, S. Kaprzyk, and J. Tobola, “Interplay of Crystal Structure Preference and Magnetic Ordering in High Entropy  $\text{CrCoFeNiAl}$  Alloys,” *Acta Physica Polonica A* **133**, 511–513 (2018).

<sup>26</sup> I R Gomersall and B L Gyorffy, “A simple theory of the electron-phonon mass enhancement in transition metal compounds,” *Journal of Physics F: Metal Physics* **4**, 1204–1221 (1974).

<sup>27</sup> B. M. Klein, L. L. Boyer, and D. A. Papaconstantopoulos, “Superconducting Properties of  $A15$  Compounds Derived from Band-Structure Results,” *Phys. Rev. Lett.* **42**, 530–533 (1979).

<sup>28</sup> I. I. Mazin, S. N. Rashkeev, and S. Y. Savrasov, “Non-spherical rigid-muffin-tin calculations of electron-phonon

coupling in high- $T_c$  perovskites,” *Phys. Rev. B* **42**, 366–370 (1990).

<sup>29</sup> B. Wiendlocha, J. Tobola, and S. Kaprzyk, “Search for  $\text{Sc}_3\text{XB}$  ( $X = \text{In, Tl, Ga, Al}$ ) perovskites superconductors and proximity of weak ferromagnetism,” *Phys. Rev. B* **73**, 134522 (2006).

<sup>30</sup> B. Wiendlocha, J. Tobola, M. Sternik, S. Kaprzyk, K. Parlinski, and A. M. Oleś, “Superconductivity of  $\text{Mo}_3\text{Sb}_7$  from first principles,” *Phys. Rev. B* **78**, 060507(R) (2008).

<sup>31</sup> Bartłomiej Wiendlocha and Malgorzata Sternik, “Effect of the tetragonal distortion on the electronic structure, phonons and superconductivity in the  $\text{Mo}_3\text{Sb}_7$  superconductor,” *Intermetallics* **53**, 150 – 156 (2014).

<sup>32</sup> W. L. McMillan, “Transition Temperature of Strongly-Coupled Superconductors,” *Phys. Rev.* **167**, 331–344 (1968).

<sup>33</sup> J. J. Hopfield, “Angular Momentum and Transition-Metal Superconductivity,” *Phys. Rev.* **186**, 443–451 (1969).

<sup>34</sup> See Supplemental Material at <http://link.aps.org/supplemental/xxxxxxx> for the discussion of the different definitions of the frequency moments, Fig. S1 and Fig. S2 for the phonon DOS plots of Nb and Ta under pressure, Fig. S3 for the XRD pattern at room temperature, and Fig. S4 for the plot of the matrix elements, which enter the formula for the McMillan-Hopfield parameters.

<sup>35</sup> S S Rajput, R Prasad, R M Singru, S Kaprzyk, and A Bansil, “Electronic structure of disordered Nb - Mo alloys studied using the charge-self-consistent Korringa - Kohn - Rostoker coherent potential approximation,” *Journal of Physics: Condensed Matter* **8**, 2929–2944 (1996).

<sup>36</sup> D. A. Papaconstantopoulos, L. L. Boyer, B. M. Klein, A. R. Williams, V. L. Moruzzi, and J. F. Janak, “Calculations of the superconducting properties of 32 metals with  $Z \leq 49$ ,” *Phys. Rev. B* **15**, 4221–4226 (1977).

<sup>37</sup> S. Massidda, Jaejun Yu, and A. J. Freeman, “Electronic structure and properties of superconducting  $\text{LiTi}_2\text{O}_4$ ,” *Phys. Rev. B* **38**, 11352–11357 (1988).

<sup>38</sup> Francis Birch, “Finite elastic strain of cubic crystals,” *Phys. Rev.* **71**, 809–824 (1947).

<sup>39</sup> Zhong-Li Liu, Ling-Cang Cai, Xiang-Rong Chen, Qiang Wu, and Fu-Qian Jing, “Ab initio refinement of the thermal equation of state for bcc tantalum: the effect of bonding on anharmonicity,” *Journal of Physics: Condensed Matter* **21**, 095408 (2009).

<sup>40</sup> G. Grimvall, *Thermophysical properties of materials* (North-Holland Publishing Company, 1986).

<sup>41</sup> Raymond Jeanloz, “Shock wave equation of state and finite strain theory,” *Journal of Geophysical Research: Solid Earth* **94**, 5873–5886 (1989).

<sup>42</sup> C. Nie, “Volume and Temperature Dependence of the Second Grüneisen Parameter of  $\text{NaCl}$ ,” *physica status solidi (b)* **219**, 241–244 (2000).

<sup>43</sup> Orson L. Anderson and Donald G. Isaak, “The dependence of the Anderson-Grüneisen parameter  $\delta_T$  upon compression at extreme conditions,” *Journal of Physics and Chemistry of Solids* **54**, 221 – 227 (1993).

<sup>44</sup> O. L. Anderson, *Equations of State for Solids in Geophysics and Ceramic Science* (Oxford University Press, New York, 1995).

<sup>45</sup> Orson L. Anderson, “Derivation of Wachtman’s Equation for the Temperature Dependence of Elastic Moduli of Oxide Compounds,” *Phys. Rev.* **144**, 553–557 (1966).

- <sup>46</sup> J. S. Dugdale and D. K. C. MacDonald, “The Thermal Expansion of Solids,” *Phys. Rev.* **89**, 832–834 (1953).
- <sup>47</sup> Y.A. Chang, “On the temperature dependence of the bulk modulus and the Anderson-Grüneisen parameter  $\delta$  of oxide compounds,” *Journal of Physics and Chemistry of Solids* **28**, 697 – 701 (1967).
- <sup>48</sup> Y. Kimura, T. Ohtsuka, T. Matsui, and T. Mizusaki, “The normal state specific heat of niobium-tantalum alloys,” *Physics Letters A* **29**, 284 – 285 (1969).
- <sup>49</sup> A. F. Guillermet and G. Grimvall, “Homology of interatomic forces and debye temperatures in transition metals,” *Phys. Rev. B* **40**, 1521–1527 (1989).
- <sup>50</sup> I. S. Grigoriev and E.Z. Meilikhov, *Handbook of physical quantities* (CRC Press New York, 1997).
- <sup>51</sup> K W Katahara, M H Manghnani, and E S Fisher, “Pressure derivatives of the elastic moduli of BCC Ti-V-Cr, Nb-Mo and Ta-W alloys,” *Journal of Physics F: Metal Physics* **9**, 773–790 (1979).
- <sup>52</sup> K.A. Jr Gschneidner, *Solid state physics* (Academic Press New York, 1964).
- <sup>53</sup> Paolo Giannozzi, Stefano Baroni, Nicola Bonini, Matteo Calandra, Roberto Car, Carlo Cavazzoni, Davide Ceresoli, Guido L Chiarotti, Matteo Cococcioni, Ismaila Dabo, Andrea Dal Corso, Stefano de Gironcoli, Stefano Fabris, Guido Fratesi, Ralph Gebauer, Uwe Gerstmann, Christos Gougousis, Anton Kokalj, Michele Lazzeri, Layla Martin-Samos, Nicola Marzari, Francesco Mauri, Riccardo Mazzarello, Stefano Paolini, Alfredo Pasquarello, Lorenzo Paulatto, Carlo Sbraccia, Sandro Scandolo, Gabriele Sclauzero, Ari P Seitsonen, Alexander Smogunov, Paolo Umari, and Renata M Wentzcovitch, “QUANTUM ESPRESSO: a modular and open-source software project for quantum simulations of materials,” *Journal of Physics: Condensed Matter* **21**, 395502 (19pp) (2009).
- <sup>54</sup> P Giannozzi, O Andreussi, T Brumme, O Bunau, M Buongiorno Nardelli, M Calandra, R Car, C Cavazzoni, D Ceresoli, M Cococcioni, N Colonna, I Carnimeo, A Dal Corso, S de Gironcoli, P Delugas, R A DiStasio Jr, A Ferretti, A Floris, G Fratesi, G Fugallo, R Gebauer, U Gerstmann, F Giustino, T Gorni, J Jia, M Kawamura, H-Y Ko, A Kokalj, E Kucukbenli, M Lazzeri, M Marsili, N Marzari, F Mauri, N L Nguyen, H-V Nguyen, A Otero de-la Roza, L Paulatto, S Ponce, D Rocca, R Sabatini, B Santra, M Schlipf, A P Seitsonen, A Smogunov, I Timrov, T Thonhauser, P Umari, N Vast, X Wu, and S Baroni, “Advanced capabilities for materials modelling with QUANTUM ESPRESSO,” *Journal of Physics: Condensed Matter* **29**, 465901 (2017).
- <sup>55</sup> Andrea Dal Corso, “Pseudopotentials periodic table: From H to Pu,” *Computational Materials Science* **95**, 337 – 350 (2014).
- <sup>56</sup> The following pseudopotentials were used: Ta.pbe-spf-n-kjpaw-psl.1.0.0.UPF and Nb.pbe-spn-kjpaw-psl.1.0.0.UPF, <http://www.quantum-espresso.org/pseudopotentials/>.
- <sup>57</sup> John P. Perdew, Kieron Burke, and Matthias Ernzerhof, “Generalized Gradient Approximation Made Simple,” *Phys. Rev. Lett.* **77**, 3865–3868 (1996).
- <sup>58</sup> G Grimvall, *The electron-phonon interaction in metals* (North-Holland Publishing Company, 1981).
- <sup>59</sup> Xiaoqing Li, “First-principles study of the third-order elastic constants and related anharmonic properties in refractory high-entropy alloys,” *Acta Materialia* **142**, 29 – 36 (2018).
- <sup>60</sup> Azkar S. Ahmad, Y. Su, S. Y. Liu, K. Ståhl, Y. D. Wu, X. D. Hui, U. Ruett, O. Gutowski, K. Glazyrin, H. P. Liermann, H. Franz, H. Wang, X. D. Wang, Q. P. Cao, D. X. Zhang, and J. Z. Jiang, “Structural stability of high entropy alloys under pressure and temperature,” *Journal of Applied Physics* **121**, 235901 (2017), <https://doi.org/10.1063/1.4984796>.
- <sup>61</sup> A. Bansil, “Coherent-potential and average  $t$ -matrix approximations for disordered muffin-tin alloys. II. Application to realistic systems,” *Phys. Rev. B* **20**, 4035–4043 (1979).
- <sup>62</sup> W. H. Butler, “Theory of electronic transport in random alloys: Korringa-kohn-rostoker coherent-potential approximation,” *Phys. Rev. B* **31**, 3260–3277 (1985).
- <sup>63</sup> B. Wiendlocha, K. Kutorasinski, S. Kaprzyk, and J. Tobola, “Recent progress in calculations of electronic and transport properties of disordered thermoelectric materials,” *Scripta Materialia* **111**, 33 – 38 (2016).
- <sup>64</sup> I.M. Lifshitz, “Anomalies of electron characteristics of a metal in the high pressure region,” *Journal of Experimental and Theoretical Physics* **11**, 1130 (1960).
- <sup>65</sup> John S. Tse, Zhiqiang Li, Kentaro Uehara, Yanming Ma, and Rajeev Ahuja, “Electron-phonon coupling in high-pressure Nb,” *Phys. Rev. B* **69**, 132101 (2004).
- <sup>66</sup> Viktor V. Struzhkin, Yuri A. Timofeev, Russell J. Hemley, and Ho-kwang Mao, “Superconducting  $T_c$  and Electron-Phonon Coupling in Nb to 132 GPa: Magnetic Susceptibility at Megabar Pressures,” *Phys. Rev. Lett.* **79**, 4262–4265 (1997).
- <sup>67</sup> S. A. Ostanin, V. Yu. Trubitsin, S. Yu. Savrasov, M. Alouani, and H. Dreyssé, “Calculated Nb superconducting transition temperature under hydrostatic pressure,” *High Pressure Research* **17**, 393–400 (2000), <https://doi.org/10.1080/08957950008245929>.
- <sup>68</sup> V K Ratti, R Evans, and B L Gyorfy, “The volume dependence of the electron-phonon mass enhancement and the pressure dependence of  $t_c$  in transition metals,” *Journal of Physics F: Metal Physics* **4**, 371–379 (1974).
- <sup>69</sup> B. Wiendlocha, M. J. Winiarski, M. Muras, C. Zvoriste-Walters, J.-C. Griveau, S. Heathman, M. Gazda, and T. Klimczuk, “Pressure effects on the superconductivity of the HfPd<sub>2</sub>Al Heusler compound: Experimental and theoretical study,” *Phys. Rev. B* **91**, 024509 (2015).
- <sup>70</sup> S. Y. Savrasov and D. Y. Savrasov, “Electron-phonon interactions and related physical properties of metals from linear-response theory,” *Phys. Rev. B* **54**, 16487–16501 (1996).
- <sup>71</sup> J. P. Carbotte, “Properties of boson-exchange superconductors,” *Rev. Mod. Phys.* **62**, 1027–1157 (1990).
- <sup>72</sup> R. Szczęśniak, A.P. Durajski, and L. Herok, “Thermodynamic properties of antiperovskite MgCNi<sub>3</sub> in superconducting phase,” *Solid State Communications* **203**, 63 – 68 (2015).
- <sup>73</sup> J. W. Garland and K. H. Bennemann, “Theory for the Pressure Dependence of  $T_c$  for Narrow-Band Superconductors,” *AIP Conference Proceedings* **4**, 255–292 (1972).